Molecular Plant Pathology

WILEY

Molecular Plant Pathology

ORIGINAL ARTICLE OPEN ACCESS

Woody Host-Specific Type III Effector HopBL2 Is Essential for *Pseudomonas savastanoi* Virulence and Associates With Plasmodesmata

Alba Moreno-Pérez[1,2,3] | Antonio Arroyo-Mateo[1,2] | Luis Rodríguez-Moreno[1,2] | Gitta Coaker[3] | Cayo Ramos[1,2]

[1]Área de Genética, Facultad de Ciencias, Campus Teatinos s/n, Universidad de Málaga, Málaga, Spain | [2]Departamento de Protección de Cultivos, Instituto de Hortofruticultura Subtropical y Mediterránea "La Mayora", Extensión Campus de Teatinos, Universidad de Málaga-Consejo Superior de Investigaciones Científicas (IHSM-UMA-CSIC), Málaga, Spain | [3]Department of Plant Pathology, University of California, Davis, Davis, California, USA

Correspondence: Cayo Ramos (crr@uma.es)

Received: 13 June 2025 | **Revised:** 15 July 2025 | **Accepted:** 5 August 2025

Funding: This research was supported by project grant PID2020-115177RB-C21 from the Spanish Ministry of Science and Innovation (MCIN)/Agencia Estatal de Investigación (AEI)/10.13039/501100011033/, the European Regional Development Fund (ERDF)–'A way to make Europe', and the National Institutes of Health (NIH) under (Grant 2R35GM136402). A. Moreno-Pérez was supported by the predoctoral (Grant FPI/BES-2015-074847) and the University of Málaga (UMA); A. Arroyo-Mateo was funded by UMA.

Keywords: HopBL | plasmodesmata | *Pseudomonas savastanoi* | *Pseudomonas syringae* | SUMO protease domain | type III effector | woody hosts

ABSTRACT

The type III secretion system in *Pseudomonas syringae* complex pathogens delivers type III effectors (T3Es) into plant cells to manipulate host processes, enhance survival, and promote disease. While substantial research has focused on herbaceous pathogens, T3Es in strains infecting woody hosts are less understood. This study investigates the HopBL family of effectors in *Pseudomonas savastanoi*, a pathogen of woody plants. HopBL1 and HopBL2, core effectors in *P. savastanoi*, are restricted to phylogroup 3 strains of the *P. syringae* complex, all isolated from woody hosts. Phylogenetic analysis suggests recent horizontal acquisition of these effectors across multiple *P. syringae* pathovars, integrated into genomic islands flanked by mobile genetic elements. Structural analysis shows that both HopBL effectors contain SUMO protease and DNA-binding domains, with HopBL1 also possessing an ethylene-responsive motif, all characteristic of XopD from *Xanthomonas* spp. Despite low sequence identity, HopBL effectors exhibit structural similarity to XopD, with HopBL1 showing greater resemblance, particularly in the arrangement of these domains. Functional assays in olive and oleander revealed strain-specific contributions of HopBL1 and HopBL2 to virulence. In oleander, the natural host of *P. savastanoi* pv. *nerii*, mutation of either effector gene resulted in reduced symptom development. We show that HopBL2 localised predominantly to subnuclear foci and associated with plasmodesmata, with partial overlap observed along microtubules, suggesting a potential role in cytoskeleton manipulation. These findings underscore the importance of T3Es unique to *P. syringae* strains infecting woody hosts and their adaptation to modulate host cellular structures to promote disease.

1 | Introduction

The ability of most gram-negative plant-pathogenic bacteria to cause disease relies on the type III secretion system (T3SS), which facilitates the translocation of type III effectors (T3Es) into plant cells. T3Es manipulate host cellular pathways to enhance bacterial survival and promote the development of disease symptoms (Büttner 2016; Xie et al. 2019; Schreiber et al. 2021). By interfering with plant immune responses, T3Es suppress both pathogen-associated molecular pattern (PAMP)-triggered

immunity (PTI) and effector-triggered immunity (ETI). PTI is initiated upon recognition of conserved bacterial features by surface-localised pattern recognition receptors (PRRs), whereas ETI is primarily mediated either through the direct recognition of T3Es by intracellular nucleotide-binding leucine-rich repeat receptors (NLRs), or by detecting the perturbations these effectors cause within the host cell (Jones and Dangl 2006; Lolle et al. 2020; Ngou et al. 2021; Yuan et al. 2021).

The functional roles of T3Es vary significantly based on their host targets, which differ in subcellular localisation and the cellular processes they influence. Key biological functions affected by T3Es include transcription, signalling, protein and RNA processing, photosynthesis, metabolism, and cytoskeleton dynamics, predominantly targeting pathways related to plant immunity (Khan et al. 2018). Advances over the past years have enhanced our understanding of effector protein functionality in bacterial pathogens of plants (Büttner 2016; Toruño et al. 2016; Khan et al. 2018; Xin et al. 2018; Bundalovic-Torma et al. 2022). While research on T3E functions in the *Pseudomonas syringae* complex has largely focused on strains infecting the model plant *Arabidopsis thaliana* and other herbaceous species (Lee et al. 2019; Laflamme et al. 2020; Bundalovic-Torma et al. 2022; Martel et al. 2022; Marín-Ponce et al. 2023; Ruiz-Bedoya et al. 2023; Lonjon et al. 2024), studies involving strains from woody hosts remain limited (Matas et al. 2014; Castañeda-Ojeda, López-Solanilla, et al. 2017; Castañeda-Ojeda, Moreno-Pérez, et al. 2017; Choi et al. 2017; Jayaraman et al. 2023; Vadillo-Dieguez et al. 2024).

The species *Pseudomonas savastanoi*, a member of phylogroup (PG) 3 within the *P. syringae* complex, comprises five pathovars responsible for the formation of knots or excrescences in woody hosts. These pathovars are *P. savastanoi* pv. *savastanoi* (Psv), pv. *nerii* (Psn), pv. *fraxini* (Psf), pv. *retacarpa* (Psr) and pv. *mandevillae* (Psm), whose strains have been isolated from olive (*Olea europaea*), oleander (*Nerium oleander*), ash, broom, and dipladenia, respectively (Caballo-Ponce et al. 2017; Moreno-Pérez et al. 2020; Caballo-Ponce et al. 2021). The effectorome of *P. savastanoi* includes 45 T3Es distributed across 34 families, as classified by Dillon, Almeida, et al. (2019), with the addition of two novel hypothetical T3Es. Among these, 24 effectors are considered core effectors, while four are exclusive to Psr, and two encode pathovar-specific truncations present in Psr and Psm (Moreno-Pérez et al. 2020; Caballo-Ponce et al. 2021). Several of these T3Es, including the core effectors HopAY1, HopAO1, HopBL1 and HopBL2, have been associated with bacterial pathogenicity in woody hosts (Matas et al. 2014; Nowell et al. 2016; Castañeda-Ojeda, Moreno-Pérez, et al. 2017; Moreno-Pérez et al. 2020).

The main regulator of the T3SS and most of its T3Es is the alternative sigma factor HrpL, which binds a highly conserved promoter motif (GGAACC-$N_{15–16}$-CCACNNA), known as the *hrp* box (Xiao and Hutcheson 1994). The HrpL-dependent expression and delivery into plant cells of HopAO1, HopBL1 and HopBL2 have been demonstrated in Psv NCPPB 3335 (Matas et al. 2014; Castañeda-Ojeda, Moreno-Pérez, et al. 2017; Moreno-Pérez et al. 2021), which serves as a model strain for investigating bacterial infection in woody hosts (Caballo-Ponce et al. 2017) and encodes 32 T3Es (Moreno-Pérez et al. 2020). These effectors inhibit early plant defence responses, including callose deposition and reactive oxygen species (ROS) production. Notably, only HopAO1 and HopBL1 suppress ETI in *Nicotiana tabacum* leaves. Additionally, HopAO1 and HopBL2, but not HopBL1, enhance the competitiveness of the effectorless polymutant *P. syringae* pv. *tomato* DC3000 D28E in planta (Matas et al. 2014; Castañeda-Ojeda, Moreno-Pérez, et al. 2017). While HopAO1 plays a crucial role in the virulence of Psv NCPPB 3335 during the infection of olive plants, the contributions of HopBL1 and HopBL2 to virulence have yet to be elucidated.

HopBL1 and HopBL2 contain a C-terminal small ubiquitin-like modifier (SUMO) protease domain (Matas et al. 2014), similar to XopD, a well-characterised effector in *Xanthomonas* spp. (Kim et al. 2013). In plants, SUMOylation orchestrates a wide range of biological functions, including growth, development and responses to environmental stimuli (Ghosh et al. 2024). Plant cells tightly regulate protein turnover through post-translational modification by ubiquitination, followed by degradation via the ubiquitin-proteasome system. T3Es from pathogens can mimic ubiquitin ligase activity, disrupting SUMOylation homeostasis in host cells to modulate innate immune responses and enhance pathogen virulence (Sharma et al. 2021). In *Xanthomonas euvesicatoria*, the causative agent of bacterial spot disease in tomato, XopD promotes bacterial proliferation and delays the onset of disease symptoms in tomato leaves (Kim et al. 2013). More specifically, XopD targets the tomato ethylene-responsive transcription factor SIERF4, thereby repressing ethylene-triggered defence-related gene expression (Kim et al. 2013) and induces transcription of bHLH132, a key transcription factor in tomato plants involved in plant growth and defence against biotic stresses (Kim and Mudgett 2019). A truncated variant of XopD found in *X. campestris* pv. *campestris* 8004, lacking the N-terminal domain, selectively targets transcription factors in *A. thaliana*, such as DELLA proteins, which are negative regulators of gibberellin signalling, and HFR1, a positive regulator of photomorphogenesis (Tan et al. 2014; Tan et al. 2015).

In this study, we analysed the distribution of *hopBL1* and *hopBL2* across a comprehensive dataset of more than 400 *P. syringae* genomes, encompassing all described pathovars within the species complex. Strikingly, both genes were exclusively found in PG3 strains isolated from woody hosts, suggesting a potential role in host specialisation. Functional assays showed that HopBL1 and HopBL2 contribute to virulence in a strain- and host-dependent manner in *P. savastanoi* isolates infecting olive and oleander plants. Subcellular localisation analysis revealed that HopBL2 accumulated predominantly in subnuclear foci and associated with plasmodesmata, with partial overlap along microtubules, suggesting that these structures may be targeted during infection of woody plants.

2 | Results

2.1 | Horizontal Acquisition of HopBL Effectors in *P. syringae* Strains From Woody Hosts

HopBL1 and HopBL2 are two of the three core T3Es identified in *P. savastanoi* strains isolated from woody hosts (Moreno-Pérez et al. 2020) and were initially reported as absent in the limited *P. syringae* genomes available from strains isolated from herbaceous hosts (Matas et al. 2014; Moreno-Pérez et al. 2020). Leveraging a dataset of over 400 sequenced

genomes (Nowell et al. 2016; Thakur et al. 2016; Dillon, Thakur, et al. 2019), we found that orthologues of one or both effectors were exclusively present in PG3 strains isolated from woody hosts (Table S1). Complete open reading frames (ORFs) of both effectors were identified in *P. syringae* pv. *eriobotryae*, *P. syringae* pv. *castaneae* ICMP 9421, and all *P. savastanoi* strains except Psm Ph3 and Psn ICMP 16944, which carry truncated versions. Several other strains encoded truncated or single effector genes, with *hopBL1*-only strains consistently isolated from woody organs, while *hopBL2*-only strains were also found in isolates from herbaceous tissues of woody hosts (Table S1). Truncated *hopBL2* variants, caused by a 1211 bp IS*52* insertion in Psm Ph3 and Psn ICMP 16944 (identified by PCR and sequencing, data not shown), along with other unverified truncated variants from additional strains (Table S1), were excluded from subsequent analyses. Sequence identity across orthologues exceeded 97% at both nucleotide and amino acid levels (Table S2), supporting recent horizontal acquisition with limited diversification.

Phylogenetic reconstruction, using XopD from *X. euvesicatoria* strain 85–10 as the outgroup, revealed that HopBL1 and HopBL2 form two distinct monophyletic clades (Figure 1a). Phylogenetic analyses using curated nucleotide alignments showed that *hopBL1* clade was split into two major subclades: the first included all four *P. savastanoi* pathovars and *Pseudomonas amygdali* CFBP 3205, while the second comprised the remaining pathovars encoding this effector. Most sequences in the *hopBL2* clade were placed into a single major subgroup, except for those from strains of *P. syringae* pv. *photiniae* and *P. syringae* pv. *ulmi*, which were isolated from herbaceous organs of woody hosts (Figure 1b, Table S1).

To explore the possibility of horizontal gene transfer, we compared the phylogenetic trees of *hopBL1* and *hopBL2* (Figure 1) with a reference tree constructed from eight housekeeping genes (Figure S1). The topology of PG3 pathovars in the housekeeping gene phylogeny closely matches that reported in previous multilocus sequence analyses (Berge et al. 2014; Baltrus et al. 2017). The *hopBL1* tree largely mirrors this phylogeny, except for *P. amygdali* CFBP 3205 and *P. syringae* pv. *rhaphiolepidis* ICMP 9756, suggesting acquisition by a PG3 ancestor, followed by loss in some strains and reacquisition through horizontal transfer. In contrast, the *hopBL2* phylogeny is incongruent with the housekeeping gene tree (Figure 1, Figure S1), indicating horizontal acquisition. Supporting these results, BLAST analyses of the *hopBL* flanking regions in *P. savastanoi* genomes revealed multiple mobile genetic elements, including tyrosine-type recombinases/integrases, transposases, and insertion sequences from the IS*3*, IS*5*/IS*1182*, and IS*66* families (Figure 2a). Furthermore, genomic island prediction based on the complete chromosome sequence of Psv NCPPB 3335 identified both effectors within genomic islands (data not shown). Together, these findings provide strong evidence for the role of horizontal gene transfer in shaping the evolution of *hopBL1* and *hopBL2* within the *P. syringae* complex.

2.2 | HopBL Effectors Feature SUMO Protease and DNA-Binding Domains

HopBL1 and HopBL2 from Psv NCPPB 3335 share approximately 65% (37% coverage) and 34% (45% coverage) amino acid identity, respectively, with XopD from *X. euvesicatoria* 85-10. Consistent with the phylogeny shown in Figure 1a, the low coverage suggests similarity is limited to specific functional domains, indicating that HopBL1 and HopBL2 are distant XopD homologues. XopD family proteins have a C-terminal SUMO protease domain (PF02902), a DNA-binding domain, and one to three ethylene-responsive element binding factor-associated amphiphilic repression (EAR) motifs (L/FDLNL/FXP) (Ohta et al. 2001; Kim et al. 2011). Both HopBL1 and HopBL2 contain the SUMO protease and DNA-binding domains, but only HopBL1 includes an EAR motif (Figure 2).

The 3D structures of HopBL1, HopBL2 and XopD were predicted using AlphaFold 3. Template modelling scores of 0.37–0.38 indicated moderate confidence in overall domain organisation, while predicted Local Distance Difference Test (pLDDT) values exceeding 90.00 for individual domains indicated high confidence in these regions. Figure 2b shows ChimeraX visualisations of the proteins with domain annotations, and Figure 2c presents per-residue confidence scores.

Superposition of the 3D structures of HopBL1, HopBL2 and XopD revealed that HopBL1 is structurally more similar to XopD than HopBL2, regarding the DNA-binding and SUMO protease domains. For the SUMO protease domain, this comparison was based on the X-ray-resolved structure of XopD (PDB ID: 5JP1), as described by Pruneda et al. (2016), and yielded a higher alignment score and lower RMSD for HopBL1–XopD (797.5; 0.52 Å over 172 atoms) than for HopBL2–XopD (394.1; 0.74 Å over 147 atoms), supporting a closer structural resemblance between HopBL1 and XopD (Figure S2).

2.3 | The Role of HopBL1 and HopBL2 in the Virulence of *P. savastanoi* Strains

To assess the contribution of HopBL effectors to the virulence of *P. savastanoi* strains, we selected the olive isolate Psv NCPPB 3335 and two oleander isolates, Psn *Psn23* and Psn CFBP 5067, all of which have been shown to induce symptoms in olive plants (Moreno-Pérez et al. 2020). Attempts to generate *hopBL1* and *hopBL2* knock-out mutants in these strains via marker exchange were unsuccessful, likely due to the presence of sequences hindering homologous recombination in the flanking regions of these genes (Figure 2a). As an alternative approach, we employed gene inactivation through plasmid insertion using an internal fragment of *hopBL1* or *hopBL2*.

The impact of *hopBL1* and *hopBL2* disruptions on virulence was initially assessed in micropropagated olive plants. At 52 days post-inoculation (dpi), the selected wild-type Psv and Psn strains induced markedly different symptoms. Knot formation was clearly visible in plants inoculated with Psv NCPPB 3335 and Psn *Psn23*, although by 52 dpi those induced by Psv NCPPB 3335 appeared slightly more necrotic (Figure S3). In contrast, knot formation was not observed in plants inoculated with Psn CFBP 5067, which developed stem swelling and a rapid necrosis that spread both upwards and downwards from the inoculation point. Disruption of *hopBL1* or *hopBL2* in Psv NCPPB 3335 did not affect knot formation, as plants inoculated with the mutants developed

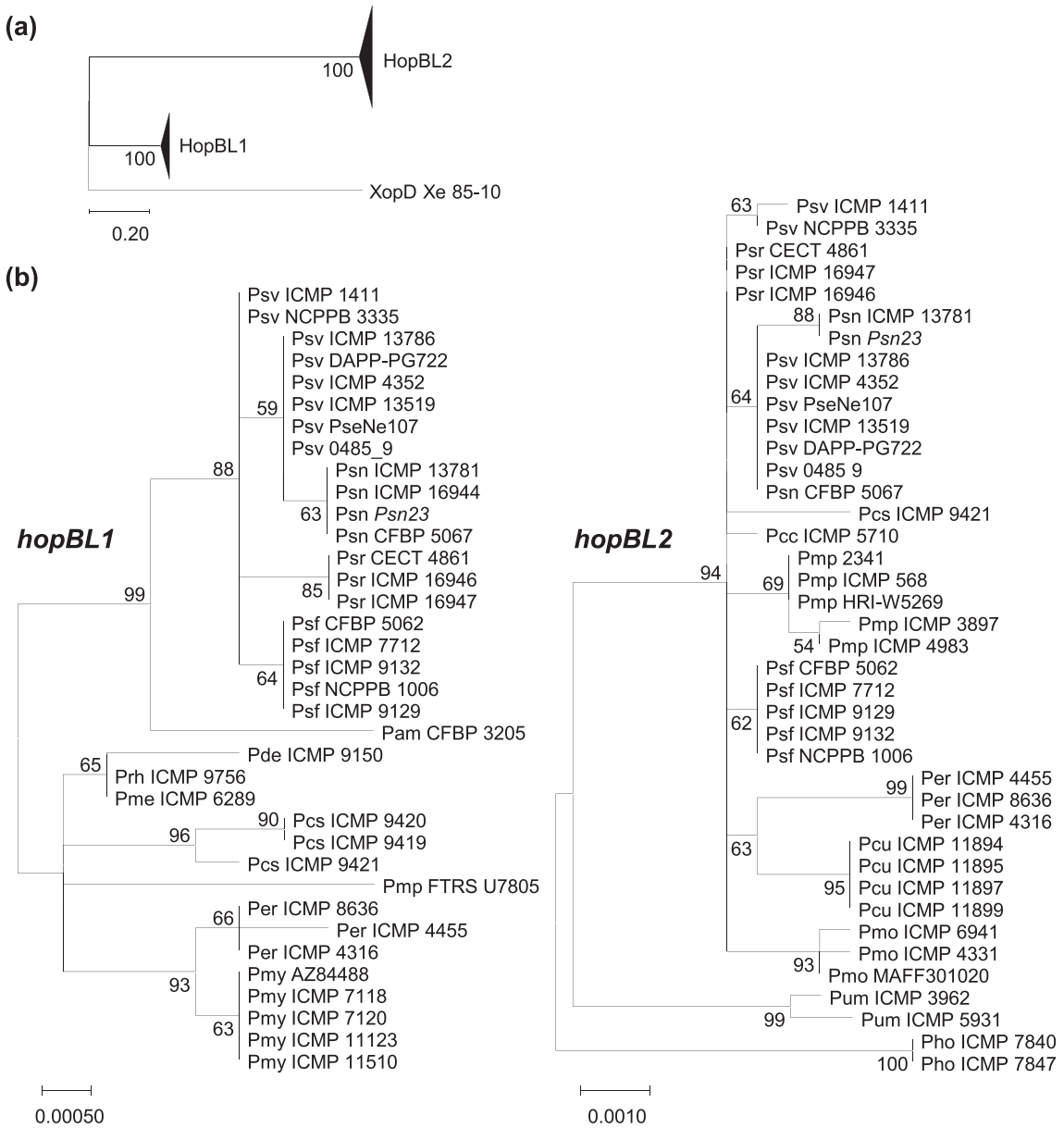

FIGURE 1 | Distribution and phylogeny of the HopBL family in the *Pseudomonas syringae* complex. (a) Maximum-likelihood phylogenetic tree of HopBL1 and HopBL2 proteins from *P. syringae* complex strains and XopD from *Xanthomonas euvesicatoria* strain 85-10. The tree was constructed using MUSCLE for sequence alignment and the maximum-likelihood method with the JTT matrix-based model. HopBL sequences included share over 80% identity and coverage with HopBL effectors from *Pseudomonas savastanoi* pv. *savastanoi* NCPPB 3335. Bootstrap values were calculated from 100 replicates. (b) Unrooted maximum-likelihood phylogenetic trees of *hopBL1* and *hopBL2* nucleotide sequences from *P. syringae* complex strains. Alignments were generated using the MUSCLE (codon) method, and trees were inferred using the maximum-likelihood method with the Kimura 2-parameter model. Bootstrap values were calculated from 1000 pseudoreplicates. Phylogenetic analyses and multiple sequence alignments were performed using MEGA X (Kumar et al. 2018). Strain names are indicated by their pathovar abbreviations (Table S1).

knots of similar size and morphology to those induced by the wild-type strain. However, plants inoculated with *hopBL1* and *hopBL2* mutants of Psn *Psn23* exhibited reduced symptom severity, with average tumour areas corresponding to approximately 45% and 73% of those induced by the wild-type strain, respectively. Although tumour size could not be quantified in plants inoculated with Psn CFBP 5067, reduced symptom severity was observed only in plants inoculated with the *hopBL2* mutant, while the *hopBL1* mutant induced symptoms indistinguishable from those caused by the wild-type strain (Figure S3). These results show that the contribution of HopBL1 and HopBL2 to the virulence of *P. savastanoi* in in vitro olive plants is strain dependent.

Given the reduced virulence of Psn *Psn23 hopBL1* and *hopBL2* mutants in micropropagated olive plants, we further investigated their role in virulence on oleander, their host of isolation. To score disease severity, we developed a semiquantitative disease phenotype scale for oleander symptoms, ranging from 0 (mock control) to 5 (maximum symptoms induced by the wild-type strain; Figure 3a). Symptoms were assessed at 90 dpi. Despite variability in symptom severity at inoculation sites infected with

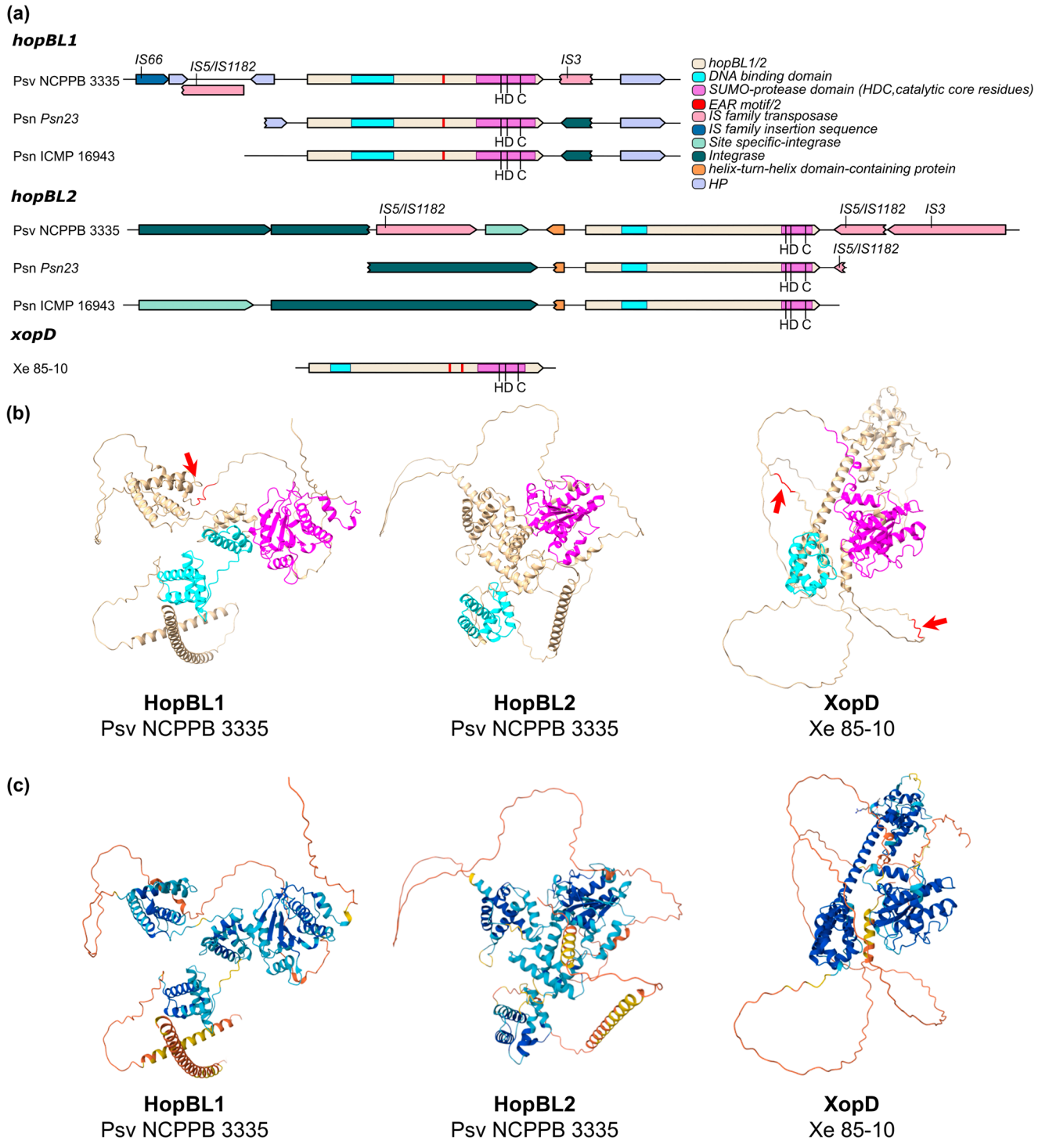

FIGURE 2 | Genomic context and predicted structures of HopBL1 and HopBL2 in *Pseudomonas savastanoi*. (a) Domain architecture of XopD from *Xanthomonas euvesicatoria* (Xe) strain 85-10, and chromosomal regions flanking the *hopBL1* and *hopBL2* genes in *P. savastanoi* pv. *savastanoi* (Psv) NCPPB 3335, pv. *nerii* (Psn) *Psn23*, and Psn ICMP 16943 strains. (b) AlphaFold-predicted 3D structures of HopBL1 and HopBL2 from Psv NCPPB 3335, and XopD from Xe 85-10, with functional domains highlighted: SUMO peptidase (magenta), DNA-binding (light blue), and ethylene-responsive element-binding factor-associated amphiphilic repression (EAR) domain (red). EAR domains are also indicated with a red arrow. (c) AlphaFold structural models coloured by per-residue confidence score based on the predicted Local Distance Difference Test (pLDDT): dark blue (pLDDT > 90), cyan (70 ≤ pLDDT ≤ 90), yellow (50 ≤ pLDDT < 70) and orange (pLDDT < 50).

the wild-type strain Psn *Psn23* (scores ranging from 1 to 5), plants inoculated with *hopBL1* or *hopBL2* mutants exhibited significantly reduced symptoms, with the reduction in virulence being more pronounced for the *hopBL1* mutant (Figure 3b). This trend was also reflected in bacterial population densities in planta: while the wild-type strains reached 10^7–10^8 colony-forming unit (CFU)/wound at the inoculation sites, the *hopBL1* mutant exhibited significantly lower populations (10^5–10^6 CFU/wound). In

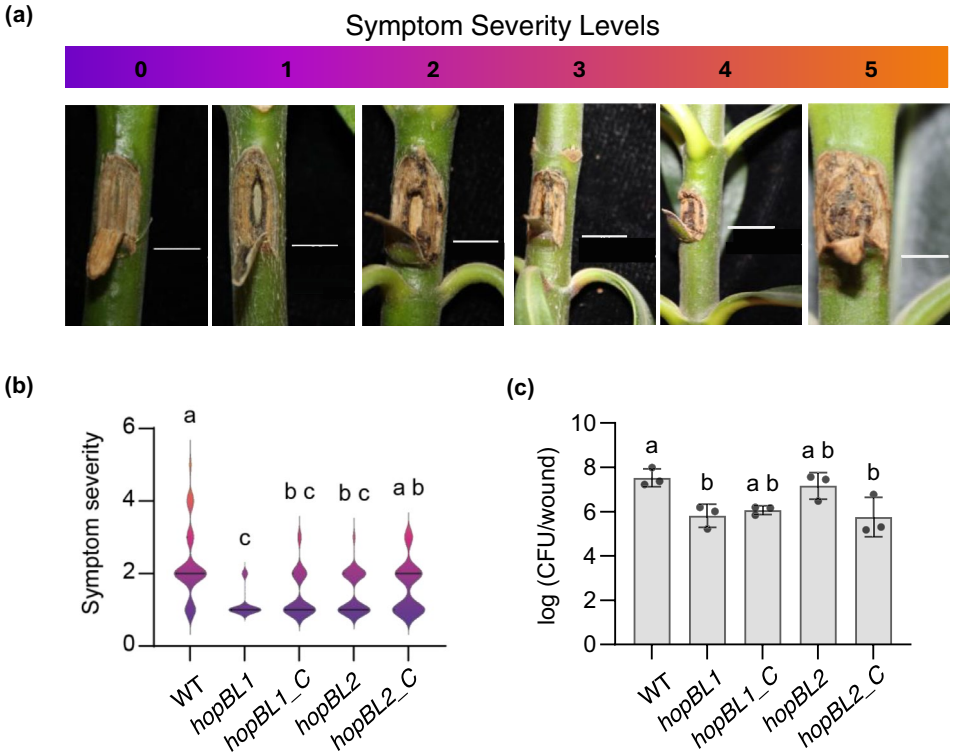

FIGURE 3 | Virulence of *Pseudomonas savastanoi* pv. *nerii Psn23 hopBL1* and *hopBL2* mutants in woody *Nerium oleander* (oleander) plants. (a) Visual scale of symptoms induced by the wild-type *Psn23* strain at 90 days post-inoculation (dpi). The scale bar represents 5 mm. A value of 0 indicates symptom levels comparable to the negative control. (b) Symptom severity at 90 dpi in plants inoculated with the indicated strains. Different letters indicate significantly different means, as determined by Kruskal–Wallis test ($p < 0.05$). (c) Bacterial populations in oleander stems at 90 dpi. Bars represent mean values from three biological replicates, with error bars indicating the standard deviation. Different letters indicate significantly different means, as determined by one-way ANOVA followed by Tukey's multiple comparisons test ($p < 0.05$). WT, wild-type *P. savastanoi* pv. *nerii Psn23; hopBL1_C, hopBL1* mutant complemented with the *hopBL1* gene; *hopBL2_C, hopBL2* mutant complemented with the *hopBL2* gene.

contrast, the *hopBL2* mutant achieved population densities comparable to the wild-type strain (Figure 3c). Complementation of *hopBL1* or *hopBL2* using a plasmid constitutively expressing these genes partially restored virulence, with *hopBL2* complementation producing symptoms more similar to those of the wild-type strain than *hopBL1* complementation. However, while *hopBL1* complementation restored bacterial populations to wild-type levels, *hopBL2* complementation unexpectedly resulted in lower populations than those of the *hopBL2* mutant and the wild-type strain (Figure 3b,c).

2.4 | HopBL2 Localises to Plasmodesmata and Associates With Microtubules in Plant Cells

To further investigate the mechanisms underlying HopBL-mediated immune suppression, we focused on HopBL2, which is structurally more distant from the well-characterised XopD and lacks the EAR motif shared by both HopBL1 and XopD (Figure 2). Although both HopBL1 and HopBL2 suppress early and late defence responses in *N. tabacum*, only HopBL2 enhances bacterial competitiveness in *Nicotiana benthamiana* (Matas et al. 2014), while its overexpression in Psn during oleander infection led to lower bacterial populations than those of the *hopBL2* mutant or the wild-type strain Psn *Psn23* (Figure 3). Together, these observations suggest a distinct and potentially host-specific mode of action for HopBL2.

To examine HopBL2 subcellular localisation, a C-terminal green fluorescent protein (GFP) fusion was expressed under the 35S promoter in *N. benthamiana* leaves by transient transformation. Western blot analysis confirmed the expression of HopBL2-GFP, with stronger accumulation observed at 24 h post-infiltration (Figure 4a). Free yellow fluorescent protein (YFP) and the plasma membrane marker LTI6B-GFP were used as controls. Confocal fluorescence microscopy revealed that HopBL2-GFP localised to the nucleus, cytoplasm and discrete punctate structures at the plasma membrane (Figure 4b). Within the nucleus, HopBL2-GFP formed subnuclear foci in the nucleoplasm but was absent from the nucleolus. At the plasma membrane, HopBL2-GFP accumulated in distinct spots resembling the localisation pattern of plasmodesmata (PD) (Thomas et al. 2008).

To determine whether HopBL2 localises to PD, we co-expressed HopBL2-GFP with the PD marker PDLP1-mCherry (Ivanov and Harrison 2014). Merged fluorescence images revealed distinct spots of HopBL2 (green fluorescence) and the PD marker (violet fluorescence), with some of these spots overlapping to produce light grey fluorescence, indicating partial colocalisation (Figure 5a,b). Quantitative fluorescence intensity analysis of two distinct colocalised puncta confirmed strong spatial overlap between HopBL2-GFP and the PD marker, providing evidence for the association of HopBL2 with plasmodesmata (Figure 5b).

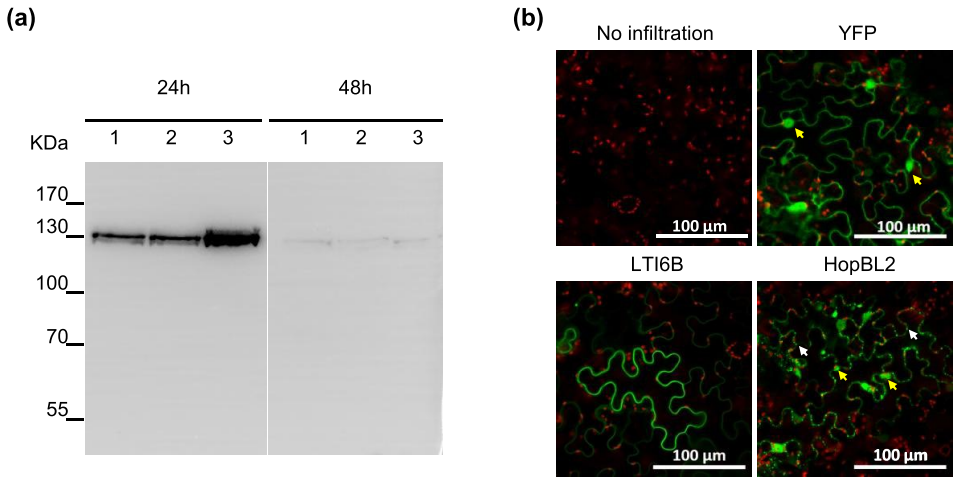

FIGURE 4 | Subcellular localisation of HopBL2 in *Nicotiana benthamiana* leaves. (a) Expression of HopBL2-GFP in *N. benthamiana* leaves at 24 and 48 h after transient expression. The numbers 1, 2, and 3 indicate three independent *Agrobacterium tumefaciens* transformants carrying the HopBL2-GFP construct. (b) Free yellow fluorescent protein (YFP), the plasma membrane marker LTI6B-GFP, and HopBL2-GFP were transiently expressed in *N. benthamiana* leaves. Cells expressing these fusion proteins were analysed 24 h post-infiltration by confocal microscopy under GFP fluorescence (green). Merged images show the overlay of GFP fluorescence and chloroplast autofluorescence (red). White arrows indicate representative punctate structures at the plasma membrane, and yellow arrows highlight nuclear localisation.

Additionally, time-lapse imaging revealed that some HopBL2-GFP puncta exhibited dynamic movement along linear trajectories within the cell (Video S1). To determine whether this movement was associated with microtubules, we co-expressed HopBL2-GFP with the microtubule marker mCherry-MAP4-MDB (Ivanov and Harrison 2014). Merged fluorescence images showed green fluorescent spots corresponding to HopBL2, violet fluorescent lines depicting microtubules, and overlapping spots indicative of colocalisation (grey fluorescence). Quantification of the fluorescence intensities from two colocalised spots revealed that, although the microtubule signal was weaker than that of HopBL2-GFP, both markers colocalised, suggesting a potential association between HopBL2 and microtubules (Figure S4).

3 | Discussion

The distribution of T3Es among *P. syringae* strains with distinct host ranges reflects their role in pathogen adaptation (Lindeberg et al. 2009; Nowell et al. 2016; Hulin et al. 2018; Moreno-Pérez et al. 2020). For instance, differences in host range between *P. syringae* pv. *glycinea* and pv. *phaseolicola* have been linked to the presence of HopC1 and HopM1 and the absence of AvrB2 (Baltrus et al. 2012). Here, we analysed the distribution of the HopBL-family effectors within the *P. syringae* complex and found that HopBL1 and HopBL2 are restricted to strains isolated from woody hosts. This pattern, consistent with Matas et al. (2014), suggests that diversification within this effector family is linked to host specialisation between herbaceous and woody plants. Furthermore, both HopBL1 and HopBL2 are exclusively detected in PG3 strains, supporting the findings of Dillon, Almeida, et al. (2019) for HopBL2. Although these authors also identified HopBL1 in the PG5 strain *P. syringae* pv. *cannabina* ICMP 2823, we excluded this sequence due to its low coverage (31%) compared to all other HopBL1 sequences analysed here, which share ≥97.8% identity (Table S2), indicating potential misannotation.

The restriction of HopBL effectors to isolates from woody hosts further supports their role in the virulence of *P. syringae* complex strains infecting these plants. Previous studies have identified similar patterns, with HopAY1 and HopAO1 significantly enriched in strains from woody hosts, while HopH3 and HopZ5 appear to have been independently acquired by multiple woody host-adapted lineages (Matas et al. 2014; Nowell et al. 2016). In our analysis, full-length *hopBL1* and *hopBL2* genes were identified in 19 *P. savastanoi* strains across all pathovars, except for Psm. Notably, the only sequenced strain from this pathovar, Psm Ph3, carries truncations in both *hopBL* genes. While *hopBL1* truncation was only observed in this strain, a truncated *hopBL2* allele was also identified in Psn ICMP 16944. In fact, PCR amplification and sequencing of *hopBL2* from these two strains and four additional Psm strains from different countries revealed that all sequences are truncated at the same position by an IS*52* element of 1211 bp (data not shown). Notably, Psn ICMP 16944 is the only Psn strain that clusters within the same phylogenetic branch as Psm Ph3 (Caballo-Ponce et al. 2021). Given that Psm strains constitute a distinct, clonal lineage closely related to Psn, the shared *hopBL2* truncation may represent convergent adaptation to *Apocynaceae* hosts. Indeed, dipladenia and oleander, the primary hosts of Psm and Psn, respectively, are the only species from this plant family to be infected by *P. savastanoi* (Caballo-Ponce et al. 2017; Caballo-Ponce et al. 2021). Additional *hopBL2* truncations were identified in eight strains isolated from hosts belonging to the *Myricaceae*, *Fagaceae*, and *Rosaceae* families (Table S1), potentially indicating a reduced functional requirement for this effector in interactions with these hosts.

The phylogenetic relationships of *hopBL1* and *hopBL2* (Figure 1), along with the genetic signatures of their flanking regions (Figure 2), suggest that these effectors have been horizontally transferred within the *P. syringae* complex. Supporting this, genomic island predictions for Psv NCPPB 3335 identified both effectors within mobile genomic regions (data not shown). Notably, PsvA, a plasmid-encoded homologue of both HopBL1

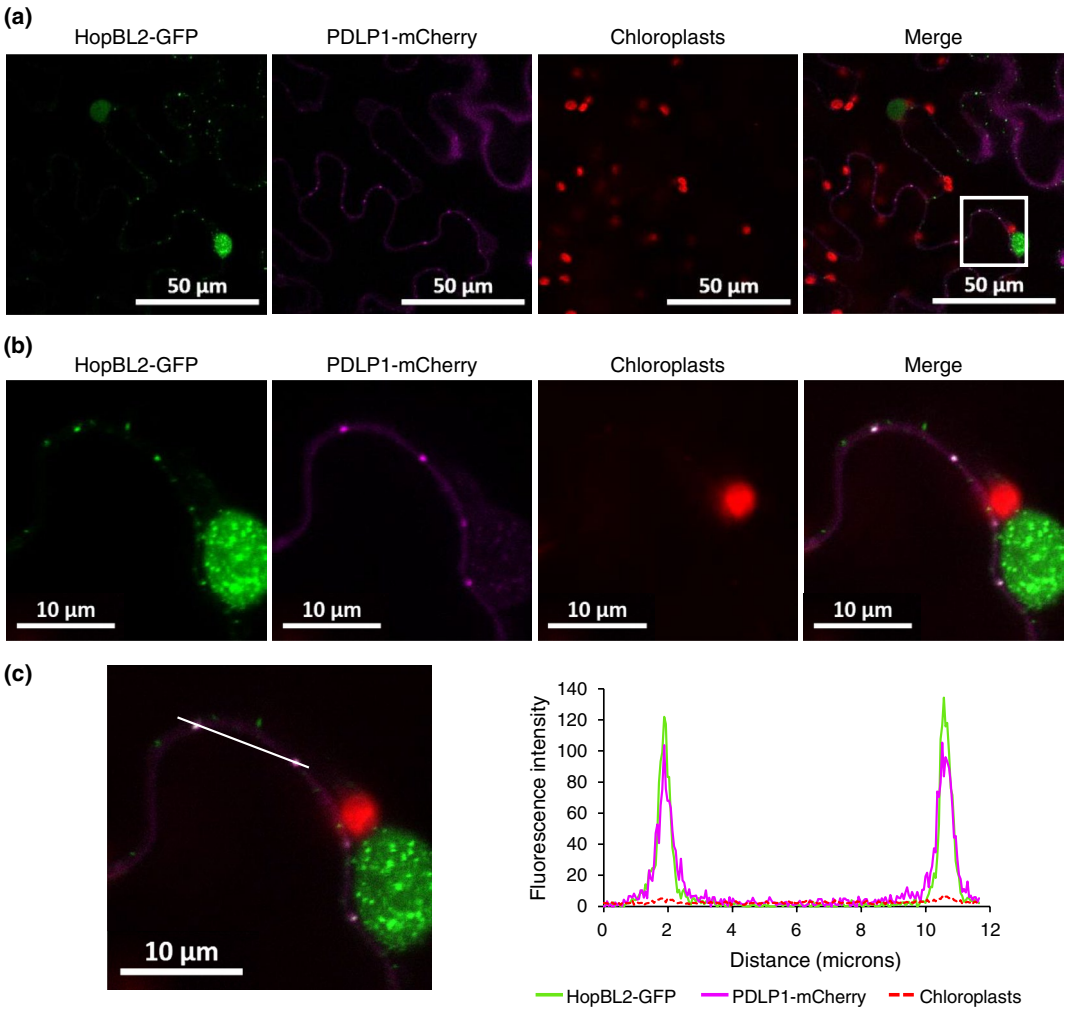

FIGURE 5 | HopBL2 partially co-localises with plasmodesmata (PD) marker protein PDLP1. HopBL2-GFP and PDLP1-mCherry fusion constructs were transiently expressed in *Nicotiana benthamiana* leaves. (a) Cells expressing the fusion proteins were analysed 24 h post-infiltration by confocal microscope under GFP fluorescence (green) and mCherry fluorescence (magenta) for PDLP1. Red autofluorescence corresponds to chloroplasts. The merged image shows the overlap of GFP, mCherry and chloroplast fluorescence. (b) Detailed view of the squared region marked in (a), highlighting the co-localisation of HopBL2 and PDLP1. (c) Graphical representation of the fluorescence intensity of GFP, mCherry and chloroplast autofluorescence along the area marked by the white line in the left image.

and XopD in *P. syringae* pv. *eriobotryae* NAE 6, is similarly flanked by an IS*5* transposase (Kamiunten 1999). In agreement with our finding, Kamiunten (1999) also identified PsvA homologues in *P. syringae* pv. *myricae* and *P. syringae* pv. *dendropanacis*, both of which cause galls on woody plants, highlighting the potential role of HopBL-family effectors in tumour formation and adaptation to woody hosts. Horizontal gene transfer plays a critical role in the evolution and diversification of T3Es in the *P. syringae* complex, enhancing pathogen adaptability and virulence. A comprehensive analysis of 24 T3E gene families in this complex revealed that while some effectors were acquired relatively recently, others have been maintained long enough to reflect the GC content and codon usage characteristic of their respective genomes (Rohmer et al. 2004). Building on this, Dillon, Almeida, et al. (2019) analysed the pan-genome of nearly 500 *P. syringae* strains from over 100 host species, tracing the evolutionary dynamics of known and putative T3Es. Their study identified multiple gene gain and loss events across effector families, underscoring the major role of horizontal gene transfer in shaping the T3E repertoire of *P. syringae*.

Consistent with Rodríguez-Moreno et al. (2008), we observed that different wild-type Psv and Psn strains induced a range of symptoms in in vitro micropropagated olive plants (Figure S3). These variations, also observed in woody olive plants infected with the same strains, likely reflect the presence of strain-specific virulence factors. Genomic analyses have revealed significant differences in the repertoire of T3E genes, type IV secretion system genes, transcription factors, and other virulence-associated genes among these strains (Moreno-Pérez et al. 2020). Such variability may contribute to the strain-dependent effects of *P. savastanoi hopBL1* and *hopBL2* disruptions observed in this study (Figure S3), and mirror patterns reported for other *P. syringae* pathovars (Sarkar et al. 2006; Ferrante et al. 2009; Lindeberg et al. 2009; Dillon, Almeida, et al. 2019). In *P. savastanoi*, strain-dependent virulence has also been described for LuxI, which is essential for full virulence in Psv DAPP-PG722 but dispensable in Psv NCPPB 3335 (Hosni et al. 2011; Caballo-Ponce et al. 2018). Furthermore, functional redundancy between HopBL1 and HopBL2 could account for the limited impact of single knockouts in Psv NCPPB 3335, where neither effector appears essential

for pathogenicity. A similar redundancy has been described for XopD in *X. euvesicatoria*, attributed to other SUMO protease effectors such as AvrRxv (Noël et al. 2002; Hotson et al. 2003; Kim et al. 2008; Kim et al. 2011). Because only single knockouts were analysed, functional compensation between HopBL1 and HopBL2 cannot be ruled out. Resolving this question would require constructing double mutants lacking both effectors and the corresponding complemented strain. However, due to recombination constraints (Figure 2), clean deletions could not be obtained, and plasmid integration mutants were used instead. Complementation of double mutants would require the stable maintenance of multiple constructs during our long-term virulence assays, likely resulting in heterogeneous bacterial populations and reduced data reliability.

In oleander, the natural host of Psn *Psn 23*, both *hopBL1* and *hopBL2* mutants caused reduced symptoms (Figure 3a,b), mirroring the requirement of PsvA for full virulence of *P. syringae* pv. *eriobotryae* NAE 6 in a different woody host, loquat (*Eriobotrya japonica*) (Kamiunten 1999). A significant decrease in bacterial populations within oleander tissues was only observed at 90 dpi for the *hopBL1* mutant (Figure 3c), suggesting a more critical role for HopBL1 in bacterial survival within oleander tissues. In *X. euvesicatoria*, XopD is also required for maximal growth in tomato leaves at the late stages of the infection, although a *xopD* mutant initially grew in planta as well as the wild-type strain (Kim et al. 2008). Because bacterial populations in Psn *Psn23*-inoculated oleander were only quantified at the end of the experiment, we cannot rule out the possibility that HopBL1 also plays a role in promoting bacterial growth specifically during the later stages of infection, similar to XopD. Time-course experiments will be necessary to address this question. Complementation of Psn *Psn23 hopBL1* or *hopBL2* mutants partially restored virulence on oleander. However, while *hopBL1* expression restored bacterial populations to wild-type levels, *hopBL2* complementation unexpectedly led to lower populations than those of both the *hopBL2* mutant and the wild-type strain (Figure 3c). As expression of the effectors in the complemented strains was driven by the constitutive P_{nptII} promoter, it is possible that altering the native expression patterns of *hopBL2* could induce physiological alterations in the bacterium, leading to a toxic effect, and/or elicit non-canonical host responses, such as triggering a hypersensitive response (ETI), any of which could contribute to the observed reduction in bacterial populations. In addition, the observed phenotype might not stem solely from expression levels but from disrupted timing of effector expression. T3Es are known to be secreted in a tightly regulated temporal cascade during infection (Park et al. 2017), and constitutive expression could interfere with this coordination. To clarify this, future experiments should complement *hopBL2* under the control of its native promoter in the mutant strain, accompanied by transcriptional analysis to monitor gene expression levels during host colonisation.

The localisation of HopBL2 to subnuclear foci observed in this study (Figure 4) aligns with the nuclear targeting of its homologue XopD in *X. euvesicatoria* (Hotson et al. 2003; Kim et al. 2013). Truncation analyses of XopD demonstrated that its N-terminal region is essential for nuclear import and speckle formation (Hotson et al. 2003). Given that HopBL2 also harbours a DNA-binding domain at its N-terminus, this region may similarly mediate its nuclear localisation. In addition to its nuclear localisation, HopBL2 forms punctate structures at the plasma membrane, partially colocalising with PDLP1 (Figure 5), a key regulator of PD function and callose deposition during plant immunity (Caillaud et al. 2014; Tee et al. 2023). Although no PD localisation signal has been identified in HopBL2, and such signals are generally poorly conserved and difficult to predict (Luna et al. 2023), its localisation pattern strongly suggests an association with PD. Consistent with this, HopBL2 was previously shown to suppress callose deposition during PTI in *N. benthamiana* (Matas et al. 2014), supporting its potential role in interfering with callose-mediated PD closure. PD closure, triggered by PTI through callose accumulation, restricts pathogen movement between plant cells (Cheval and Faulkner 2018; Liu et al. 2021; Tee et al. 2023). In response, pathogens have evolved effectors that manipulate PD permeability (Iswanto et al. 2021). For example, effectors from the plant pathogens *Phytophthora brassicae*, *Melampsora larici-populina* and *Fusarium oxysporum* suppress callose deposition or expand PD pore size to enhance pathogen spread (Germain et al. 2018; Tomczynska et al. 2020; Rahman et al. 2021; Blekemolen et al. 2022). In *P. syringae*, HopO1-1 increases PD-dependent molecular flux, facilitating bacterial infection (Aung et al. 2020). Whether HopBL2 also alters PD permeability remains to be investigated. Future studies using approaches such as PD permeability assays based on microparticle bombardment, together with interaction studies to identify host targets, may help clarify its role in association with PD.

In addition to its localisation at the plasma membrane and nucleus, HopBL2 forms dynamic, fluorescent puncta that travel along linear trajectories (Video S1), some of which colocalise with microtubules (Figure S4). Microtubules play a crucial role in plant immunity (Hardham 2013; Wang et al. 2022), and bacterial T3Es frequently target the cytoskeleton as a virulence strategy (Bhandari and Brandizzi 2020). In *P. syringae*, HopZ1a and HopAE1 interact with microtubules to suppress immunity by disrupting cytoskeletal integrity and inhibiting secretory pathways (Lee et al. 2012; Guo et al. 2016; Rufián et al. 2021). Similarly, *Ralstonia solanacearum* effectors RipU and RipAO manipulate the cytoskeleton, with RipAO causing microtubules fragmentation to impair PTI (Hiles et al. 2024; Jeon et al. 2025). In *Xanthomonas*, XopL binds microtubules to trigger cell death, further underscoring the role of cytoskeletal manipulation in bacterial virulence (Ortmann et al. 2023). Alternatively, pathogen proteins, including viral movement proteins like that of tobacco mosaic virus, target microtubules for intracellular trafficking (Kragler et al. 2003; Ouko et al. 2010; Hardham 2013). Future studies should also investigate whether HopBL2 modifies microtubule dynamics and/or utilises these networks for intracellular mobility.

In conclusion, our study reveals that HopBL1 and HopBL2 contribute to the virulence of *P. syringae* complex strains infecting woody hosts, with specific effects observed during *P. savastanoi* infection of oleander. Their phylogenetic divergence, together with the presence of genomic signatures of horizontal transfer in the proximity of *hopBL* genes, suggests that these effectors were acquired through genetic exchange and subsequently adapted to fulfil distinct roles during infection. This is further supported by their different domain architectures, including the absence

of EAR motifs in HopBL2, as well as their distinct roles in virulence. Moreover, the localisation of HopBL2 at the plasma membrane, PD, and microtubules highlights its potential to target key host cellular structures for manipulation. Given its likely involvement in modulating PD permeability, microtubule dynamics, and plant immune responses, further studies are needed to elucidate the precise molecular functions and evolutionary significance of HopBL2, and how these compare with those of HopBL1 and its *Xanthomonas* spp. homologue XopD.

4 | Experimental Procedures

4.1 | Genomic and Phylogenetic Analyses

BLAST search for *hopBL* genes and HopBL protein sequences in *P. savastanoi* genomes were identified using Geneious v7.1.13 (Kearse et al. 2012) on a curated local database comprising 21 genomes from strains isolated from woody hosts (Psf, Psm, Psn, Psv and Psr) (Moreno-Pérez et al. 2020; Caballo-Ponce et al. 2021). Additionally, HopBL paralogues from other *P. syringae* pathovars were identified and manually classified as HopBL1 or HopBL2 across 494 genomes of strains isolated from over 100 hosts (Dillon, Almeida, et al. 2019). HopBL effectors were also identified in 32 additional strains of the *P. syringae* complex. The nucleotide sequences for these effectors were extracted from a local database using Geneious v. 7.1.13 (Kearse et al. 2012), and sequences with ≥80% identity and coverage were retained for subsequent analyses (Table S1).

Multiple sequence alignments of *hopBL* genes and corresponding HopBL proteins were performed using Clustal Omega (Madeira et al. 2024). Phylogenetic analyses were conducted by refining alignments with Multiple Sequence Comparison by Log-Expectation (MUSCLE) in MEGA X (Kumar et al. 2018). For the comparison between HopBL effectors and XopD, protein sequences were used to construct a phylogenetic tree with the maximum-likelihood method and the Jones-Taylor-Thornton (JTT) substitution model (Jones et al. 1992) in MEGA X (Kumar et al. 2018). The sequences were manually curated to resolve ambiguities prior to constructing phylogenetic trees, and the tree topology was validated with 100 bootstrap replicates.

Due to high sequence similarity, individual phylogenetic trees for *hopBL1* and *hopBL2* were constructed using nucleotide sequences in MEGA X (Kumar et al. 2018). Initial trees for the heuristic search were generated automatically using the neighbour-joining (NJ) and BioNJ algorithms based on a pairwise distance matrix estimated using the maximum composite likelihood (MCL) approach. The topology with the highest log-likelihood value was selected and validated with 1000 bootstrap replicates. The *hopBL1* phylogenetic tree included 36 nucleotide sequences with a total alignment length of 2202 positions, while the *hopBL2* tree comprised 40 sequences with 2256 positions.

Phylogenetic relationships among strains harbouring HopBL effectors were further examined through multilocus sequence analysis (MLSA) of eight concatenated housekeeping genes (Table S3). Complete sequences of these genes, spanning 19,113–19,119 nucleotides per strain, were available for 53 *P. syringae* strains. Alignments were generated using MUSCLE in MEGA X (Kumar et al. 2018), and maximum-likelihood phylogenetic trees were constructed and statistically validated with 1000 bootstrap replicates.

To identify potential horizontal gene transfer events involving *hopBL* loci, BLAST analyses were conducted on ~2000 bp flanking regions upstream and downstream of the *hopBL* genes in *P. savastanoi* genomes.

4.2 | Protein Domain Identification and Structural Analyses

Domain searches for functional annotations were carried out using HHpred (Zimmermann et al. 2018; Gabler et al. 2020) and Pfam (v. 37.0) via the InterPro platform (Mistry et al. 2020). Searches for ethylene-responsive element binding factor-associated amphiphilic repression (EAR) motifs (L/FDLNL/FXP) were conducted manually as outlined by (Kim et al. 2011).

Three-dimensional (3D) structural analyses of HopBL1 and HopBL2 were performed using AlphaFold 3, which provides high-confidence predictions of inter-domain organisation and local structural domains. Confidence metrics, such as predicted template modelling scores and local distance difference tests (Abramson et al. 2024), were used to validate the predicted structures. Molecular models were visualised, refined, and superposed using ChimeraX (Pettersen et al. 2021), with structural alignments quantified using the Needleman-Wunsch algorithm (Needleman and Wunsch 1970) and root mean square deviation (RMSD) values to evaluate structural congruence at the atomic level.

4.3 | Bacterial Strain, Plasmids, and Growth Conditions

The bacterial strains and plasmids used in this study are described in Tables S4 and S5, respectively. All *P. savastanoi* strains were grown at 28°C in lysogeny broth (LB) medium (Bertani 1951) without glucose and containing 0.5% NaCl, or in Super Optimal Broth (SOB) medium (Hanahan 1983). *Escherichia coli* and *Agrobacterium tumefaciens* strains were grown in LB medium at 37°C and 28°C, respectively. When required, the medium was supplemented with the appropriate antibiotics (Table S6).

4.4 | Construction of *P. savastanoi* Mutants and Complemented Strains

To generate *P. savastanoi* mutants, the coding sequence of *hopBL1* and *hopBL2* from Psv NCPPB 3335, Psn *Psn23* and Psn CFBP 5067 (Table S4) was disrupted by chromosomal integration of the plasmids pMUTBL1 and pMUTBL2 (Table S5), respectively. These plasmids were constructed by amplifying internal fragments of *hopBL1* (1217 bp) and *hopBL2* (1058 bp) using PCR with primers listed in Table S7 and genomic DNA of Psv NCPPB 3335 as the template. The resulting PCR fragments were TA-cloned into the pCR2.1 vector (Invitrogen)

(Table S5). Plasmids were then transformed into *P. savastanoi* strains via electroporation, as previously described (Pérez-Martínez et al. 2007). Southern blotting with an *nptII* probe confirmed correct plasmid integration at target chromosomal loci. The complemented strains were constructed by transforming *hopBL1* and *hopBL2* mutants with plasmids carrying the entire coding sequences from Psv NCPPB 3335, driven by the P_{nptII} promoter (Table S5).

4.5 | Plant Infections

Virulence of *P. savastanoi* in *O. europaea* was assessed using in vitro micropropagated plants derived from a germinated cv. Arbequina seedling, rooted and maintained as described by Rodríguez-Moreno et al. (2008). Bacterial suspensions were prepared in 10 mM $MgCl_2$ at an OD_{600} of 0.1 (~10^8 CFU/mL), diluted 1:100, and 2 μL were applied to one or two stem wounds per plant (three plants per strain). Inoculated plants were kept for 52 days in a growth chamber at 25°C with a 16 h photoperiod. Symptom development was monitored using a stereoscopic microscope (MZ FLIII; Leica Microsystems). Knot area was quantified from images using QuPath 0.5.1 (Bankhead et al. 2017). A pixel classifier trained to distinguish knot from healthy tissue was applied via a custom Groovy script to calculate knot area in square pixels (pixels^2).

Virulence on oleander (*N. oleander*), accession 'Pink' (Viveros Guzmán), was tested as described by Moreno-Pérez et al. (2020). Each strain was inoculated onto three plants (10–12 wounds per plant, ~10^6 CFU per wound). Plants were maintained in a greenhouse under a natural photoperiod (15 h light/9 h dark) at 26°C/18°C (day/night). Symptoms were assessed at 90 dpi and photographed (Nikon DXM 1200 digital camera). Bacterial populations were quantified as previously described (Moreno-Pérez et al. 2020), and data analysed by ANOVA with Tukey's test ($p < 0.05$).

4.6 | Subcellular Localisation

To generate a C-terminal fusion of HopBL2 to GFP, the Gateway-compatible vector pENTR-*hopBL2* was used (Table S5). This plasmid contains the entire *hopBL2* ORF without a stop codon. The *hopBL2* gene was transferred to the Gateway destination binary vector pGWB5 (Table S5) using the Gateway LR Clonase II enzyme mix (Invitrogen). In this vector, gene expression is controlled by the 35S promoter.

For agroinfiltration experiments, two-week-old *N. benthamiana* plants were grown under controlled conditions in growth chambers at 25°C, 20% relative humidity, and a 12 h light cycle at an irradiance of 100–150 μmol/m^2/s. *A. tumefaciens* GV3101 (pMP90) strains transformed with the pGWB5 constructs were cultured overnight at 28°C in LB broth supplemented with appropriate antibiotics. After centrifugation, bacterial cells were resuspended in infiltration medium (10 mM MES pH 5.6, 10 mM $MgCl_2$ and 150 μM acetosyringone) and adjusted to an OD_{600} of 0.4. The suspensions were incubated with agitation at room temperature for 1.5–2 h prior to infiltration into *N. benthamiana* leaves using a 1 mL syringe without a needle. For co-infiltration experiments, liquid cultures of the corresponding *A. tumefaciens* strains were adjusted to an OD_{600} of 0.8 for each construct in infiltration medium and mixed in a 1:1 ratio (final OD_{600} of 0.4 per strain). Fluorescence images were taken 24 h post-infiltration using an LSM 980-Airyscan2 confocal microscope (Zeiss).

4.7 | Western Blotting

HopBL2 expression was assessed by extracting total proteins from *N. benthamiana* leaves at 24 and 48 h post-infiltration. Tissue was ground in 2× Laemmli buffer (Laemmli 1970) for protein extraction. Protein samples were separated by SDS-PAGE and immunoblotted with anti-tGFP primary antibody (1:2000) from Thermo Fisher Scientific and horseradish peroxidase-conjugated anti-rabbit secondary antibody (1:3000) from Bio-Rad. Detection was performed by chemiluminescence with SuperSignal West Femto Substrate (Thermo Fisher Scientific) and imaged with a Chemidoc system (Bio-Rad).

Author Contributions

Alba Moreno-Pérez, **Cayo Ramos**, **Gitta Coaker:** conceptualisation. **Cayo Ramos**, **Gitta Coaker**, **Luis Rodríguez-Moreno:** funding acquisition. **Cayo Ramos**, **Gitta Coaker:** project administration, resources and supervision. **Alba Moreno-Pérez**, **Cayo Ramos:** data curation. **Antonio Arroyo-Mateo**, **Alba Moreno-Pérez**, **Cayo Ramos:** formal analysis. **Antonio Arroyo-Mateo**, **Alba Moreno-Pérez:** investigation. **Antonio Arroyo-Mateo**, **Alba Moreno-Pérez**, **Cayo Ramos**, **Gitta Coaker:** methodology. **Antonio Arroyo-Mateo**, **Alba Moreno-Pérez:** software. **Cayo Ramos**, **Luis Rodríguez-Moreno**, **Gitta Coaker:** validation. **Antonio Arroyo-Mateo**, **Alba Moreno-Pérez**, **Cayo Ramos:** visualisation. **Cayo Ramos**, **Antonio Arroyo-Mateo**, **Alba Moreno-Pérez**, **Luis Rodríguez-Moreno:** writing – original draft preparation. **Alba Moreno-Pérez**, **Cayo Ramos**, **Luis Rodríguez-Moreno**, **Gitta Coaker:** writing – review and editing.

Acknowledgements

This research was supported by project grant PID2020-115177RB-C21 from the Spanish Ministry of Science and Innovation (MCIN)/Agencia Estatal de Investigación (AEI)/10.13039/501100011033/, the European Regional Development Fund (ERDF)–'A way to make Europe', and the National Institutes of Health (NIH) under grant number 2R35GM136402. A. Moreno-Pérez was supported by the predoctoral grant FPI/BES-2015-074847 and the University of Málaga (UMA); A. Arroyo-Mateo was funded by UMA. We thank J. Murillo (Universidad Pública de Navarra, Spain) for assistance with the phylogenetic analyses of HopBL sequences, and T. Toruño and S. Lolle (University of California, Davis) for support with confocal image acquisition and for providing plasmid pGB3-YFP. We are also grateful to P. García-Vallejo, A. Berrocal, and the Servicios Centrales de Apoyo a la Investigación (UMA) for their excellent technical support.

Conflicts of Interest

The authors declare no conflicts of interest.

Data Availability Statement

The data that support the findings of this study are provided in the File Supporting Information files of this article or are available from the corresponding author upon reasonable request.

References

Abramson, J., J. Adler, J. Dunger, et al. 2024. "Accurate Structure Prediction of Biomolecular Interactions With AlphaFold 3." *Nature* 630: 493–500.

Aung, K., P. Kim, Z. Li, et al. 2020. "Pathogenic Bacteria Target Plant Plasmodesmata to Colonize and Invade Surrounding Tissues." *Plant Cell* 32: 595–611.

Baltrus, D. A., H. C. McCann, and D. S. Guttman. 2017. "Evolution, Genomics and Epidemiology of *Pseudomonas syringae*." *Molecular Plant Pathology* 18: 152–168.

Baltrus, D. A., M. T. Nishimura, K. M. Dougherty, et al. 2012. "The Molecular Basis of Host Specialization in Bean Pathovars of *Pseudomonas syringae*." *Molecular Plant–Microbe Interactions* 25: 877–888.

Bankhead, P., M. B. Loughrey, J. A. Fernández, et al. 2017. "QuPath: Open Source Software for Digital Pathology Image Analysis." *Scientific Reports* 7, no. 1: 16878.

Berge, O., C. L. Monteil, C. Bartoli, C. Chandeysson, C. Guilbaud, and D. C. Sands. 2014. "A User's Guide to a Data Base of the Diversity of *Pseudomonas syringae* and Its Application to Classifying Strains in This Phylogenetic Complex." *PLoS One* 9: e105547.

Bertani, G. 1951. "Studies on Lysogenesis. I. The Mode of Phage Liberation by Lysogenic *Escherichia coli*." *Journal of Bacteriology* 62: 293–300.

Bhandari, D. D., and F. Brandizzi. 2020. "Plant Endomembranes and Cytoskeleton: Moving Targets in Immunity." *Current Opinion in Plant Biology* 58: 8–16.

Blekemolen, M. C., L. Cao, N. Tintor, et al. 2022. "The Primary Function of Six5 of *Fusarium oxysporum* Is to Facilitate Avr2 Activity by Together Manipulating the Size Exclusion Limit of Plasmodesmata." *Frontiers in Plant Science* 13: 910594.

Bundalovic-Torma, C., F. Lonjon, D. Desveaux, and D. S. Guttman. 2022. "Diversity, Evolution, and Function of *Pseudomonas syringae* Effectoromes." *Annual Review of Phytopathology* 60: 211–236.

Büttner, D. 2016. "Behind the Lines – Actions of Bacterial Type III Effector Proteins in Plant Cells." *FEMS Microbiology Reviews* 40: 894–937.

Caballo-Ponce, E., X. Meng, G. Uzelac, et al. 2018. "Quorum Sensing in *Pseudomonas savastanoi* pv. *savastanoi* and *Erwinia toletana*: Role in Virulence and Interspecies Interactions in the Olive Knot." *Applied and Environmental Microbiology* 84: e00950-00918.

Caballo-Ponce, E., J. Murillo, M. Martínez-Gil, A. Moreno-Pérez, A. Pintado, and C. Ramos. 2017. "Knots Untie: Molecular Determinants Involved in Knot Formation Induced by *Pseudomonas savastanoi* in Woody Hosts." *Frontiers in Plant Science* 8: 1089.

Caballo-Ponce, E., A. Pintado, A. Moreno-Pérez, J. Murillo, K. Smalla, and C. Ramos. 2021. "*Pseudomonas savastanoi* pv. *mandevillae* pv. nov., a Clonal Pathogen Causing an Emerging, Devastating Disease of the Ornamental Plant *Mandevilla* spp." *Phytopathology* 111: 1277–1288.

Caillaud, M.-C., L. Wirthmueller, J. Sklenar, et al. 2014. "The Plasmodesmal Protein PDLP1 Localises to Haustoria-Associated Membranes During Downy Mildew Infection and Regulates Callose Deposition." *PLoS Pathogens* 10: e1004496.

Castañeda-Ojeda, M. P., E. López-Solanilla, and C. Ramos. 2017. "Differential Modulation of Plant Immune Responses by Diverse Members of the *Pseudomonas savastanoi* pv. *savastanoi* HopAF Type III Effector Family." *Molecular Plant Pathology* 18: 625–634.

Castañeda-Ojeda, M. P., A. Moreno-Pérez, C. Ramos, and E. López-Solanilla. 2017. "Suppression of Plant Immune Responses by the *Pseudomonas savastanoi* pv. *savastanoi* NCPPB 3335 Type III Effector Tyrosine Phosphatases HopAO1 and HopAO2." *Frontiers in Plant Science* 8: 680.

Cheval, C., and C. Faulkner. 2018. "Plasmodesmal Regulation During Plant–Pathogen Interactions." *New Phytologist* 217: 62–67.

Choi, S., J. Jayaraman, C. Segonzac, et al. 2017. "*Pseudomonas syringae* pv. *actinidiae* Type III Effectors Localized at Multiple Cellular Compartments Activate or Suppress Innate Immune Responses in *Nicotiana benthamiana*." *Frontiers in Plant Science* 8: 2157.

Dillon, M. M., R. N. D. Almeida, B. Laflamme, et al. 2019. "Molecular Evolution of *Pseudomonas syringae* Type III Secreted Effector Proteins." *Frontiers in Plant Science* 10: 418.

Dillon, M. M., S. Thakur, R. N. D. Almeida, P. W. Wang, B. S. Weir, and D. S. Guttman. 2019. "Recombination of Ecologically and Evolutionarily Significant Loci Maintains Genetic Cohesion in the *Pseudomonas syringae* Species Complex." *Genome Biology* 20: 3.

Ferrante, P., C. R. Clarke, K. A. Cavanaugh, R. W. Michelmore, R. Buonaurio, and B. A. Vinatzer. 2009. "Contributions of the Effector Gene hopQ1-1 to Differences in Host Range Between *Pseudomonas syringae* pv. *phaseolicola* and *P. syringae* pv. *tabaci*." *Molecular Plant Pathology* 10: 837–842.

Gabler, F., S.-Z. Nam, S. Till, et al. 2020. "Protein Sequence Analysis Using the MPI Bioinformatics Toolkit." *Current Protocols in Bioinformatics* 72: e108.

Germain, H., D. L. Joly, C. Mireault, et al. 2018. "Infection Assays in *Arabidopsis* Reveal Candidate Effectors From the Poplar Rust Fungus That Promote Susceptibility to Bacteria and Oomycete Pathogens." *Molecular Plant Pathology* 19: 191–200.

Ghosh, S., M. Mellado Sanchez, K. Sue-Ob, et al. 2024. "Charting the Evolutionary Path of the SUMO Modification System in Plants Reveals Molecular Hardwiring of Development to Stress Adaptation." *Plant Cell* 36: 3131–3144.

Guo, M., P. Kim, G. Li, C. G. Elowsky, and J. R. Alfano. 2016. "A Bacterial Effector Co-opts Calmodulin to Target the Plant Microtubule Network." *Cell Host & Microbe* 19: 67–78.

Hanahan, D. 1983. "Studies on Transformation of *Escherichia coli* With Plasmids." *Journal of Molecular Biology* 166: 557–580.

Hardham, A. R. 2013. "Microtubules and Biotic Interactions." *Plant Journal* 75: 278–289.

Hiles, R., A. Rogers, N. Jaiswal, et al. 2024. "A *Ralstonia solanacearum* Type III Effector Alters the Actin and Microtubule Cytoskeleton to Promote Bacterial Virulence in Plants." *PLoS Pathogens* 20: e1012814.

Hosni, T., C. Moretti, G. Devescovi, et al. 2011. "Sharing of Quorum-Sensing Signals and Role of Interspecies Communities in a Bacterial Plant Disease." *ISME Journal* 5: 1857–1870.

Hotson, A., R. Chosed, H. Shu, K. Orth, and M. B. Mudgett. 2003. "*Xanthomonas* Type III Effector XopD Targets SUMO-Conjugated Proteins *in Planta*." *Molecular Microbiology* 50: 377–389.

Hulin, M. T., A. D. Armitage, J. G. Vicente, et al. 2018. "Comparative Genomics of *Pseudomonas syringae* Reveals Convergent Gene Gain and Loss Associated With Specialization Onto Cherry (*Prunus avium*)." *New Phytologist* 219: 672–696.

Iswanto, A. B. B., M. H. Vu, S. Pike, et al. 2021. "Pathogen Effectors: What Do They Do at Plasmodesmata?" *Molecular Plant Pathology* 23: 795–804.

Ivanov, S., and M. J. Harrison. 2014. "A Set of Fluorescent Protein-Based Markers Expressed From Constitutive and Arbuscular Mycorrhiza-Inducible Promoters to Label Organelles, Membranes and Cytoskeletal Elements in *Medicago truncatula*." *Plant Journal* 80: 1151–1163.

Jayaraman, J., M. Yoon, L. M. Hemara, et al. 2023. "Contrasting Effector Profiles Between Bacterial Colonisers of Kiwifruit Reveal Redundant

Roles Converging on PTI-Suppression and RIN4." *New Phytologist* 238: 1605–1619.

Jeon, H., W. Kim, and C. Segonzac. 2025. "The Disordered Effector RipAO of *Ralstonia solanacearum* Destabilizes Microtubule Networks in *Nicotiana benthamiana* Cells." *Molecules and Cells* 48: 100,167.

Jones, D. T., W. R. Taylor, and J. M. Thornton. 1992. "The Rapid Generation of Mutation Data Matrices From Protein Sequences." *Bioinformatics* 8: 275–282.

Jones, J. D., and J. L. Dangl. 2006. "The Plant Immune System." *Nature* 444: 323–329.

Kamiunten, H. 1999. "Isolation and Characterization of Virulence Gene *psvA* on a Plasmid of *Pseudomonas syringae* pv. *eriobotryae*." *Journal of Plant Pathology* 65: 501–509.

Kearse, M., R. Moir, A. Wilson, et al. 2012. "Geneious Basic: An Integrated and Extendable Desktop Software Platform for the Organization and Analysis of Sequence Data." *Bioinformatics* 28: 1647–1649.

Khan, M., D. Seto, R. Subramaniam, and D. Desveaux. 2018. "Oh, the Places They'll Go! A Survey of Phytopathogen Effectors and Their Host Targets." *Plant Journal* 93: 651–663.

Kim, J. G., K. W. Taylor, A. Hotson, M. Keegan, E. A. Schmelz, and M. B. Mudgett. 2008. "XopD SUMO Protease Affects Host Transcription, Promotes Pathogen Growth, and Delays Symptom Development in *Xanthomonas*-Infected Tomato Leaves." *Plant Cell* 20: 1915–1929.

Kim, J. G., K. W. Taylor, and M. B. Mudgett. 2011. "Comparative Analysis of the XopD Type III Secretion (T3S) Effector Family in Plant-Pathogenic Bacteria." *Molecular Plant Pathology* 12: 715–730.

Kim, J.-G., and M. B. Mudgett. 2019. "Tomato bHLH132 Transcription Factor Controls Growth and Defense and Is Activated by *Xanthomonas euvesicatoria* Effector XopD During Pathogenesis." *Molecular Plant–Microbe Interactions* 32: 1614–1622.

Kim, J.-G., W. Stork, and M. B. Mudgett. 2013. "*Xanthomonas* Type III Effector XopD Desumoylates Tomato Transcription Factor SlERF4 to Suppress Ethylene Responses and Promote Pathogen Growth." *Cell Host & Microbe* 13: 143–154.

Kragler, F., M. Curin, K. Trutnyeva, A. Gansch, and E. Waigmann. 2003. "MPB2C, a Microtubule-Associated Plant Protein Binds to and Interferes With Cell-to-Cell Transport of Tobacco Mosaic Virus Movement Protein." *Plant Physiology* 132: 1870–1883.

Kumar, S., G. Stecher, M. Li, C. Knyaz, and K. Tamura. 2018. "MEGA X: Molecular Evolutionary Genetics Analysis Across Computing Platforms." *Molecular Biology and Evolution* 35: 1547–1549.

Laemmli, U. K. 1970. "Cleavage of Structural Proteins During the Assembly of the Head of Bacteriophage T4." *Nature* 227: 680–685.

Laflamme, B., M. M. Dillon, A. Martel, R. N. D. Almeida, D. Desveaux, and D. S. Guttman. 2020. "The Pan-Genome Effector-Triggered Immunity Landscape of a Host–Pathogen Interaction." *Science* 367: 763–768.

Lee, A. H.-Y., D. P. Bastedo, J.-Y. Youn, et al. 2019. "Identifying *Pseudomonas syringae* Type III Secreted Effector Function via a Yeast Genomic Screen." *G3: Genes, Genomes, Genetics* 9: 535–547.

Lee, A. H.-Y., B. Hurley, C. Felsensteiner, et al. 2012. "A Bacterial Acetyltransferase Destroys Plant Microtubule Networks and Blocks Secretion." *PLoS Pathogens* 8: e1002523.

Lindeberg, M., S. Cunnac, and A. Collmer. 2009. "The Evolution of *Pseudomonas syringae* Host Specificity and Type III Effector Repertoires." *Molecular Plant Pathology* 10: 767–775.

Liu, J., L. Zhang, and D. Yan. 2021. "Plasmodesmata-Involved Battle Against Pathogens and Potential Strategies for Strengthening Hosts." *Frontiers in Plant Science* 12: 644870.

Lolle, S., D. Stevens, and G. Coaker. 2020. "Plant NLR-Triggered Immunity: From Receptor Activation to Downstream Signaling." *Current Opinion in Immunology* 62: 99–105.

Lonjon, F., Y. Lai, N. Askari, et al. 2024. "The Effector-Triggered Immunity Landscape of Tomato Against *Pseudomonas syringae*." *Nature Communications* 15: 5102.

Luna, G. R., J. Li, X. Wang, L. Liao, and J.-Y. Lee. 2023. "Targeting of Plasmodesmal Proteins Requires Unconventional Signals." *Plant Cell* 35: 3035–3052.

Madeira, F., N. Madhusoodanan, J. Lee, et al. 2024. "The EMBL-EBI Job Dispatcher Sequence Analysis Tools Framework in 2024." *Nucleic Acids Research* 52: W521–W525.

Marín-Ponce, L. F., C. Rodríguez-Puerto, P. Rocha-Loyola, and C. M. Rojas. 2023. "The *Pseudomonas syringae* pv. *tomato* DC3000 Effector HopD1 Interferes With Cellular Dynamics Associated With the Function of the Plant Immune Protein AtNHR2B." *Frontiers in Microbiology* 14: 1305899.

Martel, A., B. Laflamme, C. Breit-McNally, et al. 2022. "Metaeffector Interactions Modulate the Type III Effector-Triggered Immunity Load of *Pseudomonas syringae*." *PLoS Pathogens* 18: e1010541.

Matas, I. M., M. P. Castañeda-Ojeda, I. M. Aragón, et al. 2014. "Translocation and Functional Analysis of *Pseudomonas savastanoi* pv. *savastanoi* NCPPB 3335 Type III Secretion System Effectors Reveals Two Novel Effector Families of the *Pseudomonas syringae* Complex." *Molecular Plant–Microbe Interactions* 27: 424–436.

Mistry, J., S. Chuguransky, L. Williams, et al. 2020. "Pfam: The Protein Families Database in 2021." *Nucleic Acids Research* 49: D412–D419.

Moreno-Pérez, A., A. Pintado, J. Murillo, et al. 2020. "Host Range Determinants of *Pseudomonas savastanoi* Pathovars of Woody Hosts Revealed by Comparative Genomics and Cross-Pathogenicity Tests." *Frontiers in Plant Science* 11: 973.

Moreno-Pérez, A., C. Ramos, and L. Rodríguez-Moreno. 2021. "HrpL Regulon of Bacterial Pathogen of Woody Host *Pseudomonas savastanoi* pv. *savastanoi* NCPPB 3335." *Microorganisms* 9: 1447.

Needleman, S. B., and C. D. Wunsch. 1970. "A General Method Applicable to the Search for Similarities in the Amino Acid Sequence of Two Proteins." *Journal of Molecular Biology* 48: 443–453.

Ngou, B. P. M., H.-K. Ahn, P. Ding, and J. D. G. Jones. 2021. "Mutual Potentiation of Plant Immunity by Cell-Surface and Intracellular Receptors." *Nature* 592: 110–115.

Noël, L., F. Thieme, D. Nennstiel, and U. Bonas. 2002. "Two Novel Type III-Secreted Proteins of *Xanthomonas campestris* pv. *vesicatoria* Are Encoded Within the *Hrp* Pathogenicity Island." *Journal of Bacteriology* 184: 1340–1348.

Nowell, R. W., B. E. Laue, P. M. Sharp, and S. Green. 2016. "Comparative Genomics Reveals Genes Significantly Associated With Woody Hosts in the Plant Pathogen *Pseudomonas syringae*." *Molecular Plant Pathology* 17: 1409–1424.

Ohta, M., K. Matsui, K. Hiratsu, H. Shinshi, and M. Ohme-Takagi. 2001. "Repression Domains of Class II ERF Transcriptional Repressors Share an Essential Motif for Active Repression." *Plant Cell* 13: 1959–1968.

Ortmann, S., J. Marx, C. Lampe, et al. 2023. "A Conserved Microtubule-Binding Region in *Xanthomonas* XopL Is Indispensable for Induced Plant Cell Death Reactions." *PLoS Pathogens* 19: e1011263.

Ouko, M. O., A. Sambade, K. Brandner, et al. 2010. "Tobacco Mutants With Reduced Microtubule Dynamics Are Less Susceptible to TMV." *Plant Journal* 62: 829–839.

Park, E., H.-Y. Lee, J. Woo, D. Choi, and S. P. Dinesh-Kumar 2017. "Spatiotemporal Monitoring of *Pseudomonas syringae* Effectors via

Type III Secretion Using Split Fluorescent Protein Fragments." *Plant Cell* 29: 1571–1584.

Pérez-Martínez, I., L. Rodríguez-Moreno, I. M. Matas, and C. Ramos. 2007. "Strain Selection and Improvement of Gene Transfer for Genetic Manipulation of *Pseudomonas savastanoi* Isolated From Olive Knots." *Research in Microbiology* 158: 60–69.

Pettersen, E. F., T. D. Goddard, C. C. Huang, et al. 2021. "UCSF ChimeraX: Structure Visualization for Researchers, Educators, and Developers." *Protein Science* 30: 70–82.

Pruneda, J. N., C. H. Durkin, P. P. Geurink, et al. 2016. "The Molecular Basis for Ubiquitin and Ubiquitin-Like Ppecificities in Bacterial Effector Proteases." *Molecular Cell* 63: 261–276.

Rahman, M. S., M. H. Madina, M. B. Plourde, et al. 2021. "The Fungal Effector Mlp37347 Alters Plasmodesmata Fluxes and Enhances Susceptibility to Pathogen." *Microorganisms* 9: 1232.

Rodríguez-Moreno, L., A. Barceló-Munoz, and C. Ramos. 2008. "*In Vitro* Analysis of the Interaction of *Pseudomonas savastanoi* pvs. *savastanoi* and *nerii* With Micropropagated Olive Plants." *Phytopathology* 98: 815–822.

Rohmer, L., D. S. Guttman, and J. L. Dangl. 2004. "Diverse Evolutionary Mechanisms Shape the Type III Effector Virulence Factor Repertoire in the Plant Pathogen *Pseudomonas syringae*." *Genetics* 167: 1341–1360.

Rufián, J. S., J. Rueda-Blanco, D. López-Márquez, A. P. Macho, C. R. Beuzón, and J. Ruiz-Albert. 2021. "The Bacterial Effector HopZ1a Acetylates MKK7 to Suppress Plant Immunity." *New Phytologist* 231: 1138–1156.

Ruiz-Bedoya, T., P. W. Wang, D. Desveaux, and D. S. Guttman. 2023. "Cooperative Virulence via the Collective Action of Secreted Pathogen Effectors." *Nature Microbiology* 8: 640–650.

Sarkar, S. F., J. S. Gordon, G. B. Martin, and D. S. Guttman. 2006. "Comparative Genomics of Host-Specific Virulence in *Pseudomonas syringae*." *Genetics* 174: 1041–1056.

Schreiber, K. J., I. J. Chau-Ly, and J. D. Lewis. 2021. "What the Wild Things Do: Mechanisms of Plant Host Manipulation by Bacterial Type III-Secreted Effector Proteins." *Microorganisms* 9: 1029.

Sharma, M., D. Fuertes, J. Perez-Gil, and L. M. Lois. 2021. "SUMOylation in Phytopathogen Interactions: Balancing Invasion and Resistance." *Frontiers in Cell and Developmental Biology* 9: 703795.

Tan, C. M., M. Y. Li, P. Y. Yang, et al. 2015. "*Arabidopsis* HFR1 Is a Potential Nuclear Substrate Regulated by the *Xanthomonas* Type III Effector XopD(Xcc8004)." *PLoS One* 10: 18.

Tan, L., W. Rong, H. Luo, Y. Chen, and C. He. 2014. "The *Xanthomonas campestris* Effector Protein XopDXcc8004 Triggers Plant Disease Tolerance by Targeting DELLA Proteins." *New Phytologist* 204: 595–608.

Tee, E. E., M. G. Johnston, D. Papp, and C. Faulkner. 2023. "A PDLP-NHL3 Complex Integrates Plasmodesmal Immune Signaling Cascades." *Proceedings of the National Academy of Sciences of the United States of America* 120: e2216397120.

Thakur, S., B. S. Weir, and D. S. Guttman. 2016. "Phytopathogen Genome Announcement: Draft Genome Sequences of 62 *Pseudomonas syringae* Type and Pathotype Strains." *Molecular Plant–Microbe Interactions* 29: 243–246.

Thomas, C. L., E. M. Bayer, C. Ritzenthaler, L. Fernandez-Calvino, and A. J. Maule. 2008. "Specific Targeting of a Plasmodesmal Protein Affecting Cell-to-Cell Communication." *PLoS Biology* 6: e7.

Tomczynska, I., M. Stumpe, T. G. Doan, and F. Mauch. 2020. "A *Phytophthora* Effector Protein Promotes Symplastic Cell-to-Cell Trafficking by Physical Interaction With Plasmodesmata-Localised Callose Synthases." *New Phytologist* 227: 1467–1478.

Toruño, T. Y., I. Stergiopoulos, and G. Coaker. 2016. "Plant-Pathogen Effectors: Cellular Probes Interfering With Plant Defenses in Spatial and Temporal Manners." *Annual Review of Phytopathology* 54: 419–441.

Vadillo-Dieguez, A., Z. Zeng, J. W. Mansfield, et al. 2024. "Genetic Dissection of the Tissue-Specific Roles of Type III Effectors and Phytotoxins in the Pathogenicity of *Pseudomonas syringae* pv. *syringae* to Cherry." *Molecular Plant Pathology* 25: e13451.

Wang, J., N. Lian, Y. Zhang, et al. 2022. "The Cytoskeleton in Plant Immunity: Dynamics, Regulation, and Function." *International Journal of Molecular Sciences* 23, no. 15: 553.

Xiao, Y., and S. W. Hutcheson. 1994. "A Single Promoter Sequence Recognized by a Newly Identified Alternate Sigma Factor Directs Expression of Pathogenicity and Host Range Determinants in *Pseudomonas syringae*." *Journal of Bacteriology* 176: 3089–3091.

Xie, Y., X. Shao, and X. Deng. 2019. "Regulation of Type III Secretion System in *Pseudomonas syringae*." *Environmental Microbiology* 21: 4465–4477.

Xin, X.-F., B. Kvitko, and S. Y. He. 2018. "*Pseudomonas syringae*: What It Takes to Be a Pathogen." *Nature Reviews. Microbiology* 16: 316–328.

Yuan, M., B. P. M. Ngou, P. Ding, and X. F. Xin. 2021. "PTI-ETI Crosstalk: An Integrative View of Plant Immunity." *Current Opinion in Plant Biology* 62: 102030.

Zimmermann, L., A. Stephens, S.-Z. Nam, et al. 2018. "A Completely Reimplemented MPI Bioinformatics Toolkit With a New HHpred Server at Its Core." *Journal of Molecular Biology* 430: 2237–2243.

Supporting Information

Additional supporting information can be found online in the Supporting Information section. **Figure S1:** mpp70142-sup-0001-FigureS1.pdf. **Figure S2:** mpp70142-sup-0002-FigureS2.pdf. **Figure S3:** mpp70142-sup-0003-FigureS3.pdf. **Figure S4:** mpp70142-sup-0004-FigureS4.pdf. **Table S1:** mpp70142-sup-0005-TableS1.xlsx. **Table S2:** mpp70142-sup-0006-TableS2.xlsx. **Table S3:** mpp70142-sup-0007-TableS3.pdf. **Table S4:** mpp70142-sup-0008-TableS4.pdf. **Table S5:** mpp70142-sup-0009-TableS5.pdf. **Table S6:** mpp70142-sup-0010-TableS6.pdf. **Table S7:** mpp70142-sup-0011-TableS7.pdf. **Video S1:** mpp70142-sup-0012-VideoS1.avi.